ARTICLES

Synchronization and Pattern Formation in Electrochemical Oscillators: Model Calculations

Nadia Mazouz, Katharina Krischer,* Georg Flätgen, and Gerhard Ertl

Fritz-Haber-Institut der Max-Planck-Gesellschaft, Faradayweg 4-6, D-14195 Berlin (Dahlem), Germany

Received: August 30, 1996; In Final Form: December 11, 1996[⊗]

There exist many experimental examples of spatial pattern formation in electrochemical systems. Using a recently proposed model, we present numerical simulations of the spatio-temporal behavior in the bistable and oscillatory regime. The simulations reveal that for some parameter regimes only spatially inhomogeneous solutions exist. The impact of the system parameters on the spatial coupling as well as on the existence of patterns is elaborated. The predictions coincide with experimental results for a simple electrochemical reaction, the reduction of peroxodisulfate.

Introduction

The occurrence of dynamic instabilities, like, e.g., bistable or oscillatory behavior, in electrochemical systems is a widespread phenomenon. In fact, it can be expected to occur under certain conditions in nearly every electrochemical reaction. The first observations of oscillations date back to 1828,[1] and at the turn of the century Ostwald's school started its intense study. From that time on the interest in instabilities in electrochemical systems never ceased (see, e.g., the review articles in refs 2−4).

By far the most papers deal with temporal behavior only, i.e., oscillations of the total current in potentiostatic experiments or of the electrode potential under galvanostatic conditions. Directly related with this subject is the spatial state of the electrode. The oscillations originate at the electrode/electrolyte interface, and a priori there is no reason why different parts of the electrode should react synchronously. Rather, the electrode can be thought of as being composed of many local oscillators with random phase. In this case, time series of current or potential, which represent an average quantity, would exhibit a stationary value. From the fact that these global variables oscillate in time it can be deduced that there exists an efficient spatial coupling across the electrode. However, this does not imply, as it is often assumed, especially when models describing oscillatory behavior are considered, that the whole electrode oscillates in phase. It is just as well possible that coherent patterns form, and in fact there are several observations of waves accompanying current or potential oscillations. Most of them were observed in metal dissolution reactions.

The first hint that spatial structures develop during the Fe dissolution goes back to Joule[5] who observed a white film that "passed over the iron surface" at a certain phase of the oscillations, and up to now Fe remained the most thoroughly studied system not only concerning the oscillatory behavior but also in the context of spatial structures. Gerischer's first paper, a joint work with Bonhoeffer, was also devoted to oscillations;[6] Bonhoeffer and Gerischer describe waves that propagate from the rim of a disk-shaped Cu electrode to its center, a phenomenon that was later found in many other systems. During Fe dissolution it was observed that these radially symmetric waves underwent spatial period doubling bifurcations as the potential is varied.[7,8] Another interesting wave type was observed during the dissolution of a Ni wire under galvanostatic conditions.[9,10] Here, the two halves of the wire oscillated 180° out of phase, constituting a standing wave. Otterstedt et al. describe accelerated propagating activity waves during the electrodissolution of Co.[11] The formation of spiral waves was observed during the electrodeposition of Ag/Sb alloys, whereby the different regions of the patterns consist of Ag and Sb, respectively.[12−14] The introduction of the surface plasmon microscope in electrochemistry enables the observation of potential waves at two-dimensional electrodes in systems without visible changes in the surface morphology.[15] The first patterns occurring during the oscillatory reduction of $S_2O_8^{2-}$ are described in ref 16. In the same system accelerated fronts were observed in the bistable regime.[17]

From this short and not comprehensive survey it becomes apparent that in many cases dynamic instabilities manifested in current or potential time series are connected with wave phenomena. To understand when spatial structures have to be expected, model calculations are required. In ref 18 two of us presented a general, though simple, spatio-temporal model for pattern formation in electrochemical systems. The model describes systems in which convective terms, changes in surface tension, or the formation of three-dimensional surface films are not essential for the dynamic instabilities. In these cases the dominant spatial coupling is mediated via the electric potential in the electrolyte.

So far, we investigated front behavior in the bistable regime in a one-variable subset of the model where the simulations reproduced the features of the experimental data, including a most remarkable observation, namely the accelerated motion of interfaces. The acceleration could be shown to originate from a nonlocal coupling via the electrolyte. In this paper we present simulations of the full two-variable model in the bistable and oscillatory regimes. As was the case in the calculations with the one-variable model,[18,19] we again consider reactions which possess a negative differential resistance in their current potential curve, i.e., an N-shaped characteristic. This feature is often responsible for dynamic instabilities in electrochemical systems,[20] and the results here should apply to a large class of

* Author for correspondence. E-mail: krischer@fhi-berlin.mpg.de.
[⊗] Abstract published in *Advance ACS Abstracts,* March 1, 1997.

S1089-5647(96)02659-4 CCC: $14.00

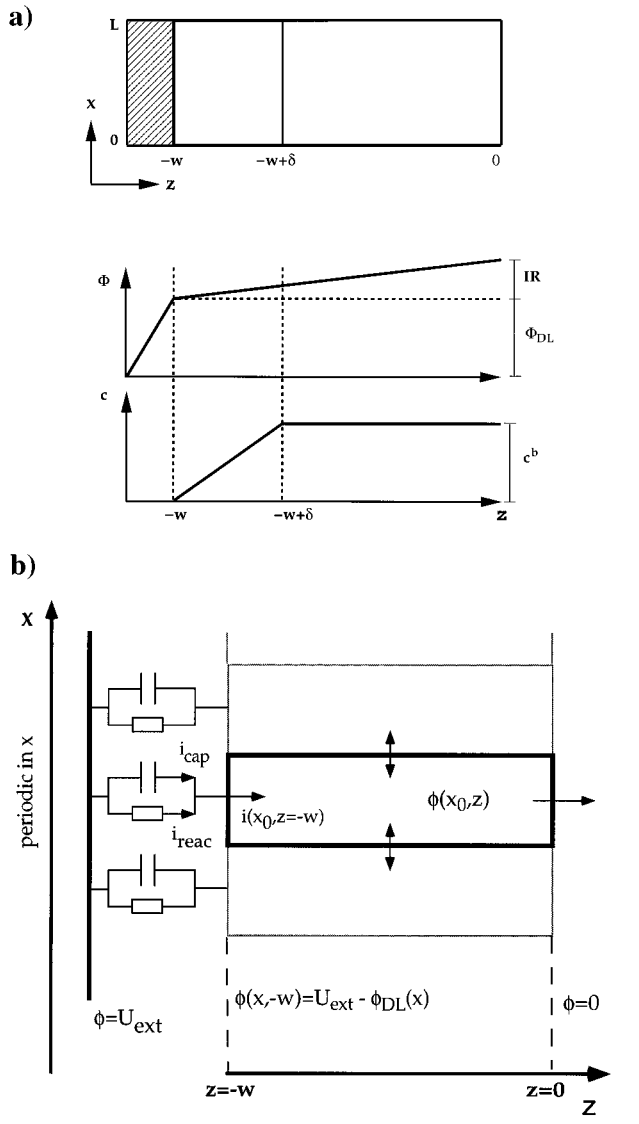

Figure 1. System configuration as well as schematics of potential and concentration distribution perpendicular to the electrode (a). Equivalent circuit (b).

electrochemical oscillators. The parameters were chosen appropriate for the reduction of $S_2O_8^{2-}$ at Ag electrodes to allow direct modeling of our experiments. After the introduction of the model and the presentation of the results, a comparison of simulations and experiments is carried out. Subsequently, the properties of the spatial coupling are discussed and the influence of the system parameters on patterns and wavelength selection is outlined.

The Model

The derivation of the model is given in ref 18. In the following we only shortly present it for the specific physical situation of a large excess of supporting electrolyte.

The variables of the system are the electric potential and the concentrations of the reacting species. We consider the simplest case, a one-dimensional electrode with periodic boundary conditions, a slightly idealized description of a ring electrode whose circumference is large compared to its thickness. As the transport of the species occurs through the electrolyte and variations in potential and concentration at the interface lead to inhomogeneous potential and concentration distributions, we deal with a spatially two-dimensional problem. The characteristic length scales involved and the nomenclature are shown in the top part of Figure 1a. The direction parallel to the electrode is called the x-direction, and L is the circumference of the electrode. We assume that perpendicular to the electrode all potential inhomogeneities are smoothed out at a distance w from the electrode, where the reference electrode is placed. Hence, in the direction perpendicular to the electrode, the z-direction, the domain extends from the end of the electrochemical double layer at $z = -w$ to the equipotential plane at $z = 0$. We restrict our examinations to potentiostatic conditions. In this case, the applied potential U_{ext} is composed of the potential drop across the double layer ϕ_{DL} and the Ohmic potential drop inside the electrolyte. We consider a reaction in which only one species is oxidized or reduced so that we have to take into account only variations of the concentration c of this species. The concentration c varies within a diffusion layer of width δ which is several orders of magnitude smaller than w and takes on its bulk value for distances larger than δ. Further, we make the approximation that the concentration profile in the z-direction can be approximated by a linear profile at any time. The bottom part of Figure 1a shows the potential and the concentration as a function of z for a homogeneous steady state.

The equivalent circuit appropriate for this geometry is shown in Figure 1b. An infinitesimal element dx of the electrode/electrolyte interface is represented by a capacitor and a non-Ohmic resistor connected in parallel; the capacitor describes the charging of this small segment dx, and the resistor possesses a current/potential characteristic of the respective reaction. The whole electrode is assumed to be composed of an infinite number of these "interface circuits" and is in contact with the electrolyte, represented by a medium with specific conductivity σ and a linear (Ohmic) current/voltage dependence. The equations for the temporal evolution of the potential and concentration at any point of the interface result from a charge and mass balance of the (charge or mass) fluxes through the boundaries of an area element dx·w.

For the particular situation of large excess of supporting electrolyte the specific conductivity is approximately constant throughout the electrolyte, and the problem is described by the following equations for the potential ϕ and the concentration c of the reactive species:

$$\Delta\phi(x,z) = 0 \tag{1}$$

and

$$c = c|_{z=-w} + (c^b - c|_{z=-w})\frac{z+w}{\delta} \qquad \text{for } -w < z \le -w+\delta$$

$$c = c^b \qquad \text{for } -w+\delta \le z \le 0 \tag{2}$$

with the time-dependent boundary conditions at the electrode

$$C_{DL}\left.\frac{\partial\phi}{\partial t}\right|_{z=-w} = i_{reac}(\phi_{DL},c) + \sigma\left.\frac{\partial\phi}{\partial z}\right|_{z=0} + \sigma\int_{-w}^{0}\frac{\partial^2\phi}{\partial x^2}\mathrm{d}z$$

$$\overset{(1)}{=} i_{reac}(\phi_{DL},c) + \sigma\left.\frac{\partial\phi}{\partial z}\right|_{z=-w} \tag{3}$$

$$\left.\frac{\partial c}{\partial t}\right|_{z=-w} = \frac{2}{nF\delta}i_{reac}(\phi_{DL},c) + \frac{2D}{\delta^2}(c^b - c|_{z=-w}) \tag{4}$$

and the additional boundary conditions

$$\begin{aligned}\phi(x+L,z,t) &= \phi(x,z,t)\\ c(x+L,z,t) &= c(x,z,t)\end{aligned} \tag{5}$$

$$U_{ext} = \phi_{DL} + \phi(z=-w) \tag{6}$$

$$\phi(x,z{=}0,t) = 0 \tag{7}$$

where $\phi(x,z)$ is the potential in the electrolyte, C_{DL} the capacitance of the electrode per unit length, σ the specific conductivity of the electrolyte, n the charge number, F Faraday's constant, and D the diffusion constant.

Laplace's equation (eq 1) describes the potential distribution inside the electrolyte. It is strictly valid where all concentrations are homogeneous, i.e., for $z > -w + \delta$. In the small region $-w < z < -w+\delta$ its solution nevertheless represents a good approximation to the true potential distribution (for a detailed discussion see ref 21 and 18). As already mentioned, the concentration varies linearly in the z-direction up to a distance δ from the working electrode (eq 2). Equations 5−7 take into account the periodic boundary condition in the x-direction, the potentiostatic operation mode, and the equipotential plane at the location of the reference electrode (or equivalently at the location of the counter electrode for small w; see discussion). The heart of the model is the equations for the temporal evolution of the potential and the concentration at the electrode (eqs 3 and 4): they are the source of all instabilities. The three terms on the right-hand side of eq 3 represent the reaction current density through the electrode at location x and the migration current densities through the infinitesimally thin "area" element $dx \cdot w$, respectively (see Figure 1b). Their sum is equal to the capacitive current density charging the double layer element dx. The concentration at the interface (eq 4) is reduced by the reaction and replenished by a diffusive transport from the bulk electrolyte to the electrode. Concentration changes due to migration can be neglected in the presence of a large amount of supporting electrolyte, and the diffusion currents parallel to the electrode are negligible compared to the other terms.

With the following dimensionless quantities

$$\phi' = \frac{nF}{RT}\phi, \quad V = \frac{nF}{RT}U_{ext}, \quad c' = \frac{c}{c^b}$$

$$t' = \frac{2D}{\delta^2}t, \quad x' = \frac{2\pi}{L}x, \quad z' = \frac{1}{w}z \qquad x \in [0,2\pi],\ z \in [-1,0]$$

where R is the gas constant and T the absolute temperature, eqs 3 and 4 become (the primes have been omitted for notational convenience)

$$\epsilon \left.\frac{\partial\phi}{\partial t}\right|_{z=-1} = \kappa c(k_1(V-\phi)^3 + k_2(V-\phi)^2 + k_3(V-\phi)) + \sigma^*\frac{L}{w}\left.\frac{\partial\phi}{\partial z}\right|_{z=-1} \tag{8}$$

$$\left.\frac{\partial c}{\partial t}\right|_{z=-1} = \kappa c(k_1(V-\phi)^3 + k_2(V-\phi)^2 + k_3(V-\phi)) + 1 - c|_{z=-1} \tag{9}$$

with

$$\sigma^* = \frac{\delta RT}{Dc_b n^2F^2}\frac{\sigma}{L}, \quad \epsilon = \frac{2C_{DL}RT}{c_b n^2F^2\delta'}, \quad \kappa = \frac{\delta k_0}{D},$$
$$k_1 = 1.826 \times 10^{-3}, \quad k_2 = -0.86, \quad k_3 = 101.98$$

where k_0 is the rate constant and the polynomial in eqs 8 and 9 represents the dimensionless reaction current density which exhibits an N-shaped characteristic; the coefficients were optimized for the reduction of peroxodisulfate under conditions that we investigated experimentally.

For a given potential distribution at the electrode, $\phi(x,z{=}-1,t)$, together with eqs 5 and 7 Laplace's equation can be solved analytically:

$$\phi(x,z,t) = \sum_{n=1}^{\infty}(\tilde{A}_n(z,t)\cos[nx] + \tilde{B}_n(z,t)\sin[nx]) + \tilde{A}_0(z,t) \tag{10a}$$

with z and t dependent coefficients

$$\tilde{A}_0(z,t) = za_0(t), \quad \tilde{A}_n(z,t) = \sinh\left[2\pi n\frac{w}{L}z\right]a_n(t)$$
$$\tilde{B}_n(z,t) = \sinh\left[2\pi n\frac{w}{L}z\right]b_n(t) \tag{10b}$$

Further we expand the concentration at the electrode, $c(x,z{=}-1,t)$, by a Fourier series

$$c(x,z=-1,t) = \sum_{n=0}^{\infty}(C_n(t)\cos[nx] + D_n(t)\sin[nx]) \tag{11}$$

Substituting eqs 10 and 11 into eqs 8 and 9 leads to an infinite set of ordinary differential equations for the temporal evolution of the coefficients $A_i(t) = -\tilde{A}_i(z{=}-1,t)$ and and $B_i(t) = -\tilde{B}_i(z{=}-1,t)$ for the potential at the electrode

$$\epsilon\frac{dA_0}{dt} = -\kappa f_0(A_i,B_i,C_i,D_i) - \sigma^*\frac{L}{w}A_0 \tag{12a}$$

$$\epsilon\frac{dA_n}{dt} = -\kappa f_n(A_i,B_i,C_i,D_i) - \sigma^*\cdot 2\pi n\coth\left(\frac{w}{L}2\pi n\right)A_n \tag{12b}$$

$$\epsilon\frac{dB_n}{dt} = -\kappa f_n(A_i,B_i,C_i,D_i) - \sigma^*\cdot 2\pi n\coth\left(\frac{w}{L}2\pi n\right)B_n \tag{12c}$$

and for the temporal evolution of the coefficients $C_i(t)$ and $D_i(t)$ for the concentration at the electrode

$$dC_0/dt = \kappa f_0(A_i,B_i,C_i,D_i) + 1 - C_0 \tag{13a}$$

$$dC_n/dt = \kappa f_n(A_i,B_i,C_i,D_i) - C_0 \tag{13b}$$

$$dD_n/dt = \kappa f_n(A_i,B_i,C_i,D_i) - D_n \tag{13c}$$

where the functions $f_n(A_i,B_i,C_i,D_i)$ represent the projection of the reaction current density i_{reac} onto the coefficient space.

The global current density can be easily obtained using eq 10:

$$i_{tot} = -\frac{1}{2\pi}\frac{\sigma^*L}{2\pi w}\int_0^{2\pi}\left.\frac{\partial\phi}{\partial z}\right|_{z=-1}dx = \frac{-\sigma^*}{2\pi}\frac{L}{w}A_0 \tag{14}$$

i_{tot} is a function of the homogeneous mode A_0 only, as all contributions of the inhomogeneous modes cancel each other when intergrating over the whole electrode.

In the numerical simulations, eqs 12−13 were integrated with the Livermore solver for ordinary differential equations (lsode)[22] using 2×73 nontrivial cosine and sine modes for each variable. The functions f_n were evaluated in physical space, whereby $3\times2\times(73+1)$ collocation points were used for the FFT back into the coefficient space.[23]

Results

In the spatially homogeneous case, eqs 1−7 reduce to a system of two ordinary differential equations which are equivalent to models derived for the temporal behavior of the $S_2O_8^{2-}$ reduction[24] and the reduction of In^{3+} in the presence of SCN^-,[25] two reactions that exhibit an N-shaped current−potential characteristic. Roughly speaking, such a characteristic leads to bistable behavior for high resistance, large overvoltage, and fast transport (small δ), and it exhibits oscillatory behavior if

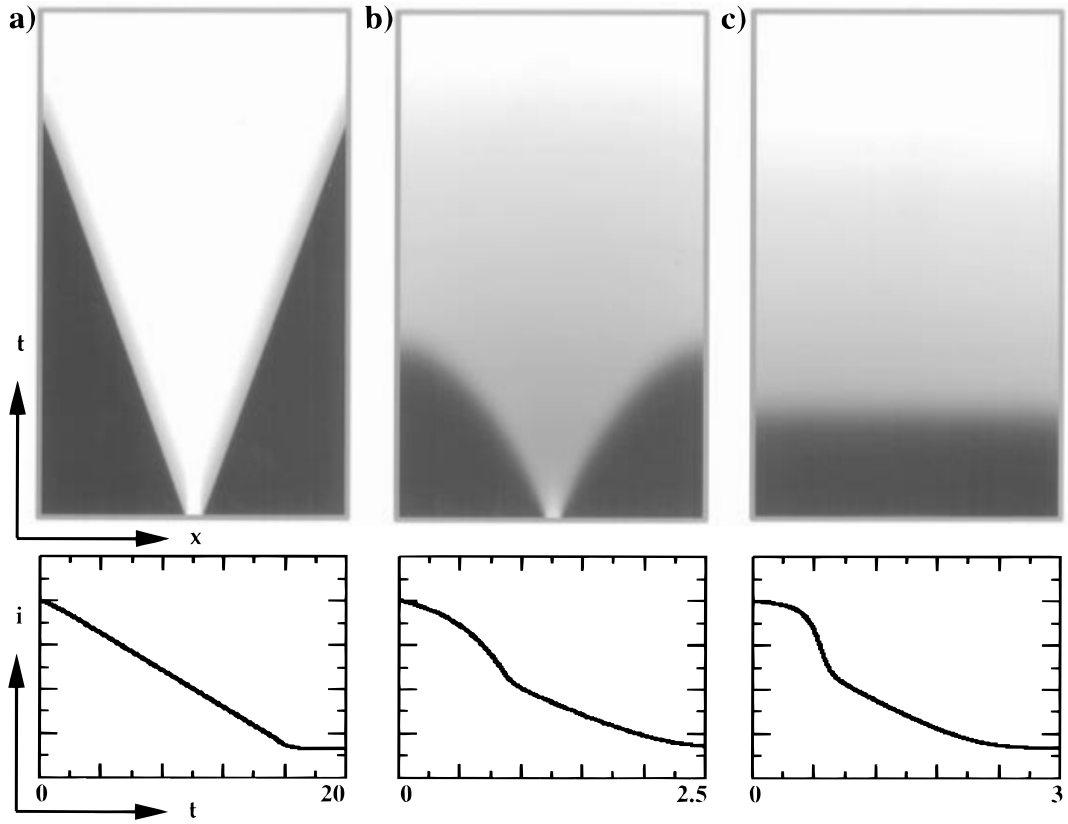

Figure 2. Gray scale representation of the spatiotemporal evolution of the potential at $z = -w$ (above) and time series of the global current (below) in the bistable regimes for three values of w/L: (a) $w/L = 0.053$, $\sigma^* = 2.6 \times 10^{-5}$; (b) $w/L = 1.59$, $\sigma^* = 7.96 \times 10^{-4}$; and (c) $w/L = 47.7$, $\sigma^* = 2.38 \times 10^{-2}$; remaining parameters: $V = -500$, $\epsilon = 1.8 \times 10^{-4}$. $\kappa = 0.006$ for both cases.

resistance, overvoltage and transport are lowered. In the following, we investigate the behavior of the system for spatially inhomogeneous perturbations. Thereby we concentrate on three parameter sets of the homogeneous system in the bistable and oscillatory regime. Our main interest is how the behavior is influenced by a change in the spatial coupling. The coupling is described by the second terms of eq 8 or eqs 12b and 12c. Obviously, there are two parameters that affect the coupling, σ^* and w/L. σ^* can be considered as a dimensionless conductivity and w/L is the ratio of the distance between working and reference electrode and the length of the electrode, respectively.

Figure 2 displays three transitions in the bistable regime for different coupling parameters. In all three cases, the electrode was initially set in the steady state with the lower current density, with a small nucleus in the high current state. From left to right we increased both w/L and σ^* such that the homogeneous steady states remained unchanged. For small values of w/L (Figure 2a) we obtain a picture that is familiar from reaction−diffusion systems;[1] the transition is mediated via fronts that move with constant velocity. If w/L becomes larger, the transition is still accompanied by sharp interfaces; however, the propagation velocity of the interfaces increases with time (Figure 2b). Moreover, the electrode does not evolve to the active steady state immediately behind the interface. For still larger values of w/L, the initial perturbation is readily distributed across the whole electrode which then relaxes homogeneously to the other state (Figure 2c). The qualitative difference of the transitions is also reflected in the global current densities. In Figure 2a the global current density represents the relative portions of the electrode in the two stationary states at any time. In the case of large w/L (Figure 2c), the global current density is totally determined by the kinetics of the reaction, Figure 2b being an intermediate case. (Note the different time scales.) As the kinetic is always autocatalytic, it can be concluded that whenever a linear increase in the current density is observed, the transition occurs via fronts.

Figure 3 displays two more complex situations that correspond to experimental data reported in ref 16. Figure 3a is obtained in the so-called "complex bistable" regime where the behavior can only be understood taking into account the second variable, i.e., in our case the concentration. In Figure 3a one of the stable fixpoints is a focus. The initial conditions were chosen as in Figure 2, and similarly to Figure 2b an accelerated front propagates across the electrode followed by a relatively homogeneous transient. A comparison of the spatiotemporal plot with the global current density reveals that while the front is observed, the global current density steadily increases, overshooting its stationary value toward which it slowly relaxes while the spatial transient is nearly uniform. Adjusting the parameters such that the system becomes oscillatory but is still close to the bistable regime, the spatiotemporal behavior changes only slightly (Figure 3b). The oscillations of the global current density have a strong relaxation-like character. The fast increase of the global current density is connected with frontlike waves, and the slower decrease as well as the quasi-stationary phase is associated with nearly invisible spatial modulations. Though the spatial modulations appear to be weak, the system will never acquire a homogeneously oscillating state, as the latter is linearly unstable with respect to spatial perturbations, and the state shown represents the long-term behavior.

Increasing the distance to the saddle-node bifurcation, the patterns in the oscillatory regime become more diverse. Figure 4 shows how global current density (Figure 4a) and spatiotemporal behavior (Figure 4b) change upon increasing L (which enters into σ^* and w/L) for an oscillatory state close to the Hopf bifurcation. In the first two time series in Figure 4a and spatiotemporal plots in Figure 4b, the parameters were chosen such that the homogeneous oscillation is still stable and has just become unstable respectively. In both cases, a small

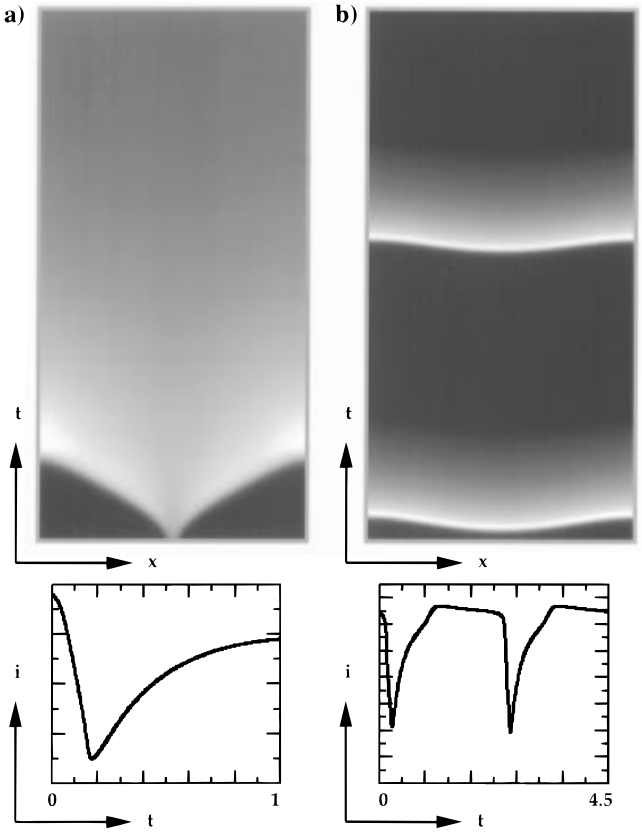

Figure 3. Gray scale representation of the spatiotemporal evolution of the potential at $z = -w$ (above) and time series of the global current (below) in the complex bistable (a) and oscillatory regime (b): (a) $w/L = 0.32$, $V = -300$, $\sigma^* = 1.33 \times 10^{-3}$, $\epsilon = 0.001$; (b) $w/L = 0.04$, $V = -270$, $\sigma^* = 2.55 \times 10^{-4}$, $\epsilon = 0.001$. $\kappa = 0.02$ for both cases.

sinusoidal perturbation was added to the homogeneous limit cycle. In the first case, the perturbation is damped out, whereas it grows in the second one. (With linear stability analysis we checked that the homogeneous oscillation is indeed unstable.) This spatially inhomogeneous attractor can be viewed as a superposition of a homogeneous oscillation and a standing wave with wavenumber one (i.e., just one wavelength fits into the system). Thus, this bifurcation cannot be detected from a measurement of the global current density (Figure 4a). This is not the case when L is increased further: In the third time series in Figure 4a the current density shows quasi-periodic behavior, indicating that the homogeneous mode is changing with time. The corresponding spatiotemporal picture exhibits an amplitude-modulated standing wave (not shown). Upon still further increasing L, the time series of the current density become steadily more complex, the qualitative changes being always accompanied by more complex spatial patterns. This means that not just the homogeneous mode but also some inhomogeneous modes are involved in the corresponding bifurcations.

The fifth time series in Figure 4a becomes irregular after a long nearly periodic transient. Despite this aperiodic behavior of the global current, the corresponding spatiotemporal picture (third plot in Figure 4b) has a surprising coherent appearance with a clear dominance of the wavenumber two. For slightly larger electrodes a regular pattern with the wavenumber two stabilizes (6th time series in Figure 4a and third plot in Figure 4b). Hence, the simulations give the impression that the system tries to form patterns with a characteristic wavelength. For intermediate electrode lengths, i.e., lengths that are close to neither one wavelength nor two wavelengths, the system reacts in a complex manner.

We are still in the very beginning of investigations of the patterns in the oscillatory regime. Our preliminary results on even larger electrodes or smaller ratios w/L indicate that the formation of regular patterns with higher wavenumbers becomes more and more unlikely, and an irregular behavior is favored, though a characteristic length is still discernible. An extreme case is shown in the last example of Figure 4, a and b, respectively.

Discussion

Comparison with Experiments. The parameters in the simulations were chosen appropriate for the reduction of $S_2O_8^{2-}$ at Ag electrodes in the bistable and oscillatory regime, and hence, the simulations can be compared with experimental findings published recently.[16] However, before we start to compare experiments and simulations, we would like to point out that the experiments in ref 16 were done with a disk-shaped electrode, while the simulations are based on a "quasi one-dimensional" electrode geometry. Therefore, we can only expect that gross features are captured.

In ref 16 three cases are discussed that correspond to three of the parameter sets studied here, a transition in each, the bistable and the "complex bistable" case, and a simple periodic oscillation. The transition in the *bistable regime* was found to be accompanied by accelerating fronts whereby the interface width is in the range of 0.1−0.5 mm. The corresponding simulation is shown in Figure 2b, reproducing both the acceleration as well as the front width. The experimental data in the *complex bistable* and oscillatory regime exhibit two time scales and two length scales. The fast time scale is determined by the dynamics of the potential, whereas the slow time scale corresponds to the slower dynamics of the reacting species. Generally, frontlike behavior was found in parallel to the rapid changes with typical interface widths close to the one in the bistable regime, whereas during the slow "recovery" of the system only weak, nearly homogeneous variations were discernible. Thus, in the complex bistable regime potential fronts travel across the surface while the current density increases, which is followed by a slow relaxation to the steady state.[26] A comparison with the corresponding simulations displayed in Figure 3a shows that these qualitative features are reproduced in the simulations. However, the slow relaxation might be accompanied by a wave emerging from the rim of the electrode (see, e.g., Figure 9 in ref 16). This second wave does not exist in the simulations and is most likely a result of the inhomogeneous potential distribution at disk electrodes.[27]

In the *oscillatory regime* the experimental picture shown in[16] resembles the complex bistable case, i.e., the spatio-temporal behavior is composed of a front-like structure that travels quickly across the electrode and a slow, more or less, homogeneous relaxation to the original state. Again, these features are reproduced in the calculations (Figure 3b). Beyond that, the calculations reveal that the homogeneous oscillation is unstable, a fact that is difficult to prove experimentally and that points once more to the necessity to interpret the dynamics in terms of spatial and temporal instabilities.

Influence of σ^* and w/L on Spatial Coupling and Pattern Formation. The comparison between experiments and simulations shows that the model reproduces the main features of the experiments. To comprehend why the patterns form and in order to be able to predict when and what type of patterns occur, it is necessary to understand the mechanism of the spatial coupling and especially, the influence of the two parameters σ^* and w/L on the coupling.

The coupling occurs through the electrolyte, more precisely through migration currents in the electrolyte. They are determined by the potential distribution in the electrolyte, which in turn depends on the parameter w/L (eq 10). To see how w/L

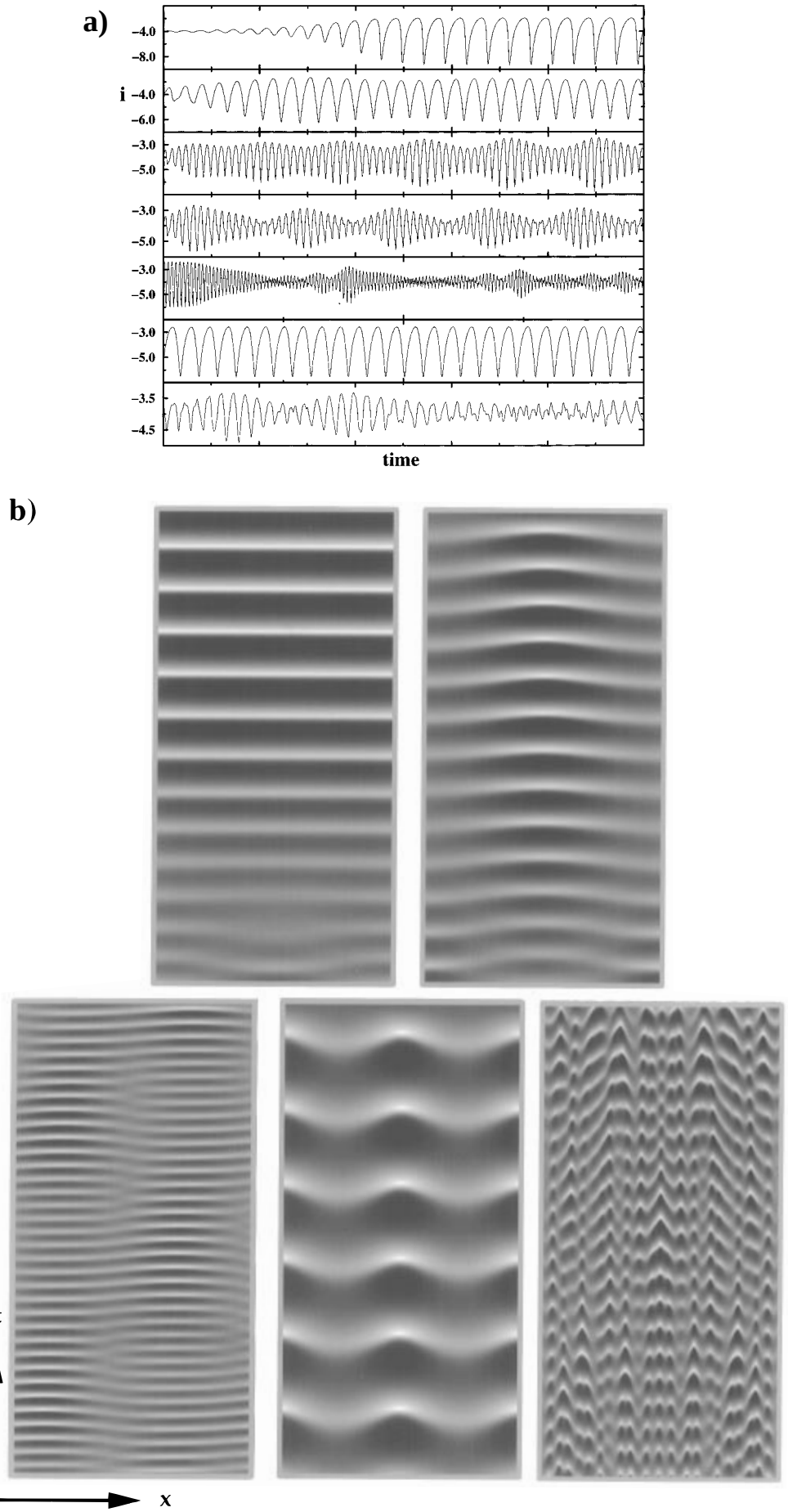

Figure 4. (a) Time series of the global current for different values of σ^* and w/L. From top to bottom: $w/L = 0.159$, $\sigma^* = 0.001\,59$, $w/L = 0.095$, $\sigma^* = 0.000\,95$; $w/L = 0.087$, $\sigma^* = 0.000\,87$; $w/L = 0.0$, $\sigma^* = 0.000\,73$; $w/L = 0.068$, $\sigma^* = 0.000\,68$; $w/L = 0.053$, $\sigma^* = 0.000\,53$; $w/L = 0.0047$, $\sigma^* = 0.000\,047$; total time shown: $t = 20$, $t = 50$, $t = 50$, $t = 100$, $t = 20$, $t = 30$; remaining parameters: $V = -247$, $\epsilon = 0.001$, $\kappa = 0.02$. (b) Gray scale representation of the spatiotemporal evolution of the potential at $z = -w$ corresponding to *the first two and last three cases* of (a). (In (b) only a section of (a) is shown.)

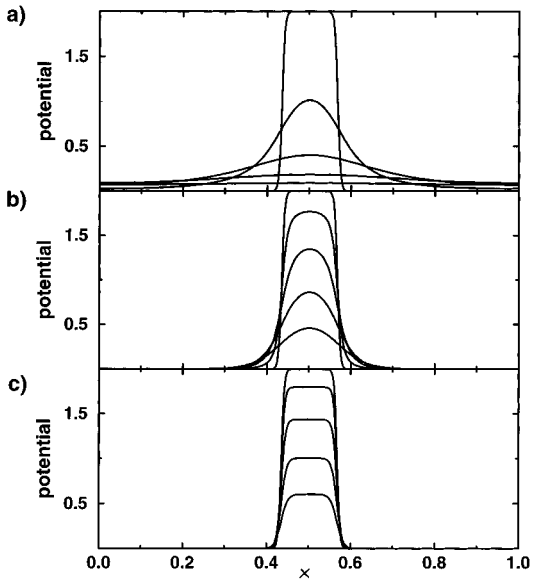

Figure 5. Potential distribution as a function of x for 5 locations z_i in the electrolyte and three values of w/L: for (a) $w/L = 0.64$, for (b) $w/L = 0.08$, and for (c) $w/L = 0.016$. $z_i = -1, -0.9, -0.8, -0.7, -0.6$; note that the case of $z_i = -1$ is at the position of the electrode, i.e., the initial condition chosen.

influences the potential distribution in the electrolyte, let us assume that there is a small rectangular perturbation at the electrode similar to the initial conditions in the simulations in Figures 2 and 3. If we represent this potential distribution as a Fourier series, a considerable number of modes is excited. From eq 10 it follows that the contributions of all coefficients of the Fourier series decrease with increasing distance from the electrode. The higher the mode number, the more rapid the decrease of the corresponding coefficient. Hence, a sharp structure at the electrode becomes broader in its lateral dimension and smaller in amplitude with progressive distance from the electrode. The delocalization of a sharp structure at the electrode into the electrolyte can be seen in Figure 5 where this effect is pronounced for large arguments of sinh, i.e., for large w/L (Figure 5a). If on the other hand the electrode is large compared to w, the argument of the sinh becomes small, and the potential distribution at the electrode decays nearly linearly into the electrolyte. Accordingly, structures at the electrode are preserved in the electrolyte (cf. Figure 5b,c). Hence, the ratio w/L determines the amount of delocalization of an inhomogeneous potential distribution at the electrode into the electrolyte.

At a certain position x_0, the potential in the whole domain between working and reference electrolyte reacts on the temporal evolution of the potential drop at this position $(\mathrm{d}\phi(x_0)/\mathrm{d}t)|_{z=-w}$. This means that due to the interplay of Laplace's equation (1) and boundary condition (3), a perturbation of the potential at x_0 is felt even at a position far away from x_0. In other words, the spatial coupling is nonlocal, defined by a characteristic distance (range) over which the state of the system at one point influences other parts of the system with a distance-dependent strength. From the arguments above it follows that the parameter w/L determines the *range* of the coupling; for large values w/L the coupling is of long range, whereas for small values w/L it becomes short range or local.

Now, let us consider σ^*. This quantity appears in front of the spatial operator in eqs 12b and 12c. Consequently, it determines the *strength* of the coupling, i.e., the characteristic time of the coupling with respect to the characteristic time of the reaction term. What makes things complicated is that the homogeneous mode also depends on σ^* and w/L, and accordingly none of the parameters can be varied independently without modifying the homogeneous steady states. Note, however, that the dependence of σ^* on L results from the normalization of the electrode to one. It tells us that the strength of the coupling is equally affected upon increasing the conductivity or reducing the length of the electrode. Hence, in experiments the strength of the coupling is not a function of the electrode length, implying that the range of the coupling can be varied independently by varying L (which is of course not a favorable parameter to change experimentally). In contrast, also in the dimensional form there are no parameters available that affect the coupling strength without affecting the homogeneous steady states at the same time.

With these considerations the simulations shown in Figure 2 can be interpreted. In the calculations w/L was tuned while keeping the homogeneous steady states constant, i.e., adjusting σ^* correspondingly. Hence strength as well as range increases from left to right in Figure 2. The transition from fronts with constant velocity to accelerated fronts can be traced back to an increase of the coupling range. This effect is more and more superimposed by the influence of the increasing strength. If the coupling strength is high, a perturbation of the electrode potential at some position spreads out quickly. As a consequence, the range of points that are affected by this perturbation becomes larger on the time scale of the reaction. In an extreme case this leads to a completely synchronized behavior as shown in Figure 2c. The difference between an apparent long-range coupling through a high strength and the long-range coupling discussed above is described in ref 19. Implications of it, like the existence of accelerated fronts with sharp interfaces, are only visible for low coupling strength.

Under galvanostatic conditions the homogeneous steady states do not depend on the potential drop in the electrolyte and thus are not influenced by the two coupling parameters σ^* and w/L. Hence, in these systems the effect of the long-range coupling can be studied separately from the effect of the coupling strength by changing w, which is experimentally much easier than changing L. Regarding the effect of w, we would like to point out that a prerequisite of the model is the existence of an equipotential line at a distance w from the working electrode. Of course, a reference electrode measures the potential at a point in the electrolyte, and only if the reference electrode is far enough from the electrode can one assume that at the position of the reference electrode the potential is independent of x. Locating the reference electrode close to the working electrode, as is often done with the help of a Luggin capillary, the potential drops between different positions of the working electrode and the reference electrode are different, and hence our model is not strictly applicable. However, an equipotential plane close to the working electrode can be realized if instead of the reference electrode the counter electrode is brought close to the working electrode. Therefore, whenever we say that the range depends on the distance between working and reference electrode, this is to be understood as the distance between working electrode and an equipotential line which can also be provided by the counter electrode. In refs 9 and 10, Lev et al. describe patterns that were obtained with an experimental setup in which the counter electrode was located close to the working electrode.

Another important result of our calculations is that in the oscillatory regime complex patterns may develop. For the parameters in the simulations the patterns have a characteristic wavelength of about 3 cm. From the experimental data in ref 16, the same size was estimated, which is larger than electrodes generally used in experiments. In ref 16 the electrodes had diameters of 6−8 mm, and the full spatiotemporal behavior could only be reconstructed from several successive images,

whereby the patterns themselves exhibited only relatively simple structures. However, as already pointed out, the wavelength depends on the ratio of reaction constant and coupling strength. For higher reaction constants the wavelength becomes smaller, and the scenario presented in Figure 4 should be observable. The time series of the global current density (Figure 4a) demonstrate that in many bifurcations leading to a more complex spatial behavior the homogeneous mode is involved. Therefore, caution is required when concluding from measured time series on the dynamics of the homogeneous state. We consider it to be likely that some of the reported transitions of mixed-mode and aperiodic oscillations result from spatiotemporal bifurcations.

Conclusions

Dynamic instabilities in electrochemical systems are often associated with symmetry breaking in both time and space. Increasing the specific conductivity of the electrolyte and the distance between working and reference electrode tends to synchronize different parts of the electrode up to the complete destruction of any spatial structure. In contrast, whenever reference or counter electrodes are close to the working electrode, the formation of spatial patterns is favored.

References and Notes

(1) Fechner, M. G. Th. *Schweiggers J. Phys. Chem.* **1828**, *53*, 129.
(2) Wojtowicz, J. In *Modern Aspects of Electrochemistry*; Bockris, J. O. Conway, B. E. Eds.; Butterworth: London, 1973.
(3) Hudson, J. L.; Tsotsis, T. T. *Chem. Eng. Sci.* **1994**, *49*, 1493.
(4) Koper, M. T. M. In *Advances in Chemistry Physics;* Prigogine,I., Rice. S. A. Eds.; John Wiley & Sons, Inc.: New York, 1996.
(5) Joule, J. P. *Philos. Mag.* **1844, *24***, 106.
(6) Bonhoeffer, K. F.; Gerischer, H. *Z. Elektrochem.* **1948**, *52*, 149.
(7) Hudson, J. L.; Tabora, J.; Krischer, K.; Kevrekidis, I. G. *Phys. Lett. A* **1993**, *179*, 355.
(8) Sayer, J. C.; Hudson, J. L. *Ind. Eng. Chem. Res.* **1995**, *34*, 3246.
(9) Lev, O.; Sheintuch, M.; Pismen, L. M.; Yarnitzky, Ch. *Nature* **1988**, *336*, 488.
(10) Lev, O.; Sheintuch, M.; Yarnitsky, H.; Pismen, L. M. *Chem. Eng. Sci.* **1990**, *45*, 839.
(11) Otterstedt, R. D.; Jaeger, N. I.; Plath, P. J. *Int. J. Bifurcation Chaos* **1994**, *4*, 1265.
(12) Raub, E.; Schall, A. *Z. Metallkunde* **1938**, *30*, 149.
(13) Krastev, I..; Nikolova, M.; Nakada, I. *Electrochim. Acta* **1989**, *34*, 1219.
(14) Krastev, I.; Koper, M. *Physica A* **1995**, *213*, 199.
(15) Flätgen, G.; Krischer, K.; Pettinger, B.; Doblhofer, K.; Junkes, H.; Ertl, G. *Science* **1995**, *269*, 668.
(16) Flätgen, G.; Krischer, K.; Ertl, G. *J. Electrocanal. Chem.* **1996**, *409*, 183.
(17) Flätgen, G.; Krischer, K. *Phys. Rev. E* **1995**, *51*, 3997.
(18) Flätgen, G.; Krischer, K. *J. Chem. Phys.* **1995**, *103*, 5428.
(19) Mazouz, N.; Flätgen, G.; Krischer, K.; Ertl, G. *Phys. Rev. E*, in press.
(20) Koper, M. T. M. *Electrochim. Acta* **1992**, *37*, 1771.
(21) Newman, J. In *Adv. Electrochem. Electrochem. Eng.* **1967**, *5*.
(22) Hindmarsh, A. C. *ACM-SIGNUM Newslett.* **1980**, *15*, 10.
(23) Canuto, C.; Quarteroni, A.; Hussaini, M.; Zang, T. A. *Spectral Methods in Fluid Dynamics*; Springer: Berlin, 1988.
(24) Wolf, W.; Ye, J.; Purgand, M.; Eiswirth, M.; Doblhofer, K. *Ber. Bunsen-Ges. Phys. Chem.* **1992**, *96*, 1797.
(25) Koper, M. T. M.; Sluyters, J. H. *J. Electroanal. Chem.* **1991**, *303*, 73.
(26) In ref 16 we proposed that the concentration changes monotonically during the transition. In the simulations shown in Figure 3 the concentration exhibits the same qualitative behavior as the potential which we now believe is also the case in the experiment. However, this change in interpretation does not affect the conclusions drawn in ref 16 about length and time scales in this regime which are in accordance with the simulations.
(27) J. Newman, *J. Electrochem. Soc* **1966**, *113*, 1235.